

# Kinetic studies in a batch reactor using ion exchange resin catalysts for oxygenates production: Role of mass transfer mechanisms

Viviana M.T.M. Silva<sup>1</sup>, Alírio E. Rodrigues\*

Laboratory of Separation and Reaction Engineering (LSRE), Department of Chemical Engineering, Faculty of Engineering, University of Porto, Rua Dr. Roberto Frias s/n, 4200-465 Porto, Portugal

Received 2 March 2005; received in revised form 31 May 2005; accepted 8 July 2005  
Available online 24 August 2005

## Abstract

Oxygenated compounds are usually produced by a reversible liquid phase reaction using ion exchange resins with a bidisperse pore structure as catalyst. Mass transport is mainly controlled by diffusion through the macropores and the mass transfer resistance in the gel microspheres is negligible. Therefore, in this paper a mathematical model of the batch reactor considering diffusion of the species in the external film and then macropore diffusion inside the particle and reaction in the gel microspheres was developed. The numerical solution is implemented through the numerical package PDECOL and detailed explanations of the procedure used are presented. The model was applied to the diethylacetal synthesis using ethanol and acetaldehyde as reactants and Amberlyst 18 as catalyst. The experimental data are fitted with a two-parameter model based on a Langmuir–Hinshelwood rate expression in order to get the true reaction kinetics. The influence of the mass transfer mechanisms is evaluated in terms of the effectiveness factor history during the transient state of the batch reactor. The values of the effectiveness factor calculated at equilibrium with the batch reactor model are compared with those calculated from a steady state infinite bath model.

© 2005 Elsevier Ltd. All rights reserved.

**Keywords:** Oxygenated compounds; Ion exchange resins; Mass transfer limitations; Effectiveness factor; Orthogonal collocation

## 1. Introduction

Most industrial chemical processes are catalytic, and therefore the importance and economical significance of catalysis is enormous. More than 80% of the present industrial processes established since 1980 in the fine chemical, petrochemical and biochemical industries use catalysts (Tirronen and Salmi, 2003; Chaudhari and Mills, 2004). The increasing demand for liquid fuels is the driving force for the petroleum industry. However, there is a growing interest in reducing dependence on petroleum and increasing the use of renewable resources for fuel and organic chemicals

production (Embree et al., 2001). To satisfy high performance engines and more and more strict exhaust emission standards, modern gasoline and diesel must meet given specifications which can vary from country to country. The octane and cetane ratings are one of the most known measures of gasoline and diesel quality, respectively. In order to achieve an acceptable octane number, oxygenates like methyl tertiary-butyl ether (MTBE), ethyl tertiary-butyl ether (ETBE) or tertiary amyl methyl ether (TAME) are added to gasoline to ensure clean combustion. Acetals, and particularly diethylacetal, have been under consideration as oxygenated additives to diesel fuel because they drastically reduce the emission of particles and NO<sub>x</sub> while keeping or improving the cetane number and helping in the combustion of the final products, without decreasing the ignition quality (Boennohoff, 1980, 1983; Golubkov and Golubkov, 2002; Laborde, 2003). These oxygenate compounds are commonly produced by a liquid phase reversible

\* Corresponding author. Tel.: +351 22 5081671; fax: +351 22 5081674.

E-mail addresses: viviana@fe.up.pt (V.M.T.M. Silva),

arodrig@fe.up.pt (A.E. Rodrigues).

<sup>1</sup> On temporary leave from School of Technology and Management, Bragança Polytechnic Institute, Campus de Santa Polónia, Apartado 1134, 5301-857 Bragança, Portugal.

Table 1  
Some experimental investigations of oxygenates production in the literature using acid ion exchange resins

Source	Experimental apparatus	Product	Catalyst
Ali and Bhatia (1990)	Fixed bed catalytic reactor	MTBE	A15
Rehfinger and Hoffmann (1990)	Continuous stirred tank reactor	MTBE	A15
Caetano et al. (1994)	Continuous stirred tank reactor	MTBE	A18
Zhang and Datta (1995)	Upflow integral reactor, continuous	MTBE	A15
Fite et al. (1994)	Differential tube reactor	ETBE	Lewatit K2631
Oost and Hoffmann (1996)	Continuous flow recycle reactor	TAME	Lewatit SPC 118
Fite et al. (1998)	Continuous upflow packed-bed reactor	MTBE	Bayer K2631
Ziyang et al. (2001)	Fixed bed catalytic reactor	MTBE	A15
Pääkkönen and Krause (2003)	Continuous stirred tank reactor	TAME	A16, A35, XE586
Boz et al. (2004)	Fixed bed catalytic reactor	TAEE	A15
Ferreira and Loureiro (2004)	Batch stirred tank reactor	TAME	A15

reaction in acid medium. Because standard ion exchange resins are insoluble acids, they can be used with advantage in many organic reactions where an acidic catalyst is required. Special macroporous sulphonic resins are used for oxygenates production, as shown in Table 1.

Catalysis with acid ion exchange resins has the following advantages over the use of liquid acids:

- a higher local concentration of  $H^+$  ions;
- no corrosion;
- possibility of use in continuous processes;
- less secondary reactions;
- easy separation from the reaction medium.

The macroreticular ion exchange resins show bidisperse pore distribution (Quinta-Ferreira and Rodrigues, 1993; Caetano et al., 1994; Ihm et al., 1996). Macroporous resins are characterized by micropores of 0.5–2 nm and macropores of 20–60 nm, depending on the degree of cross-linking (de Dardel and Arden, 2002). The reactant species should first diffuse through the macropores to the external surface of microspheres and then penetrate into the gel phase.

The adsorption and reaction processes over catalysts with bidisperse pore size distribution have been widely studied in the literature. The heterogeneous catalysis processes are regulated by transport phenomena (external and internal diffusion), the adsorption and the reaction at the solid surface. The mass transfer effects in bidisperse catalysts are due to three main mechanisms: mass transfer of species between the bulk fluid phase and the external surface of the stationary phase particles (external mass transfer); diffusive migration through the pores inside the particles (internal pore diffusion); and surface diffusion. The internal pore diffusion may occur by molecular diffusion and Knudsen diffusion (for gas phase), depending on pore size, adsorbate concentrations and other conditions. For resins the microspheres are a gel phase and therefore the mass transfer mechanism that should be considered is the gel diffusion, as shown in Fig. 1.

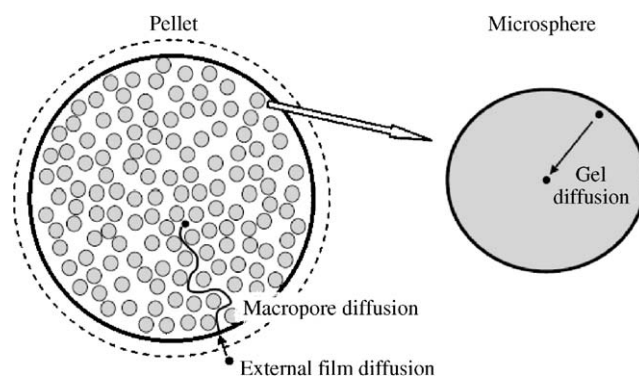


Fig. 1. Schematic representation of the mass transfer mechanisms in a particle of a resin with bidisperse pore structure.

Many authors have developed several models to describe the transport phenomena inside a particle with a bidisperse pore structure. The first and more used model was developed by Ruckenstein et al. (1971), who considers a spherical macroporous pellet to be an assembly of small microspheres. The adsorbate diffuses into macropores, adsorbs on the macropore walls, and also diffuses into the micropores and is adsorbed there. Recently, this model was used to determine the effectiveness of bidisperse catalysts (Leitão et al., 1994), to study adsorption induced convection in the macropores of a bidisperse adsorbent particle (Taqvi et al., 1997). Later, an equivalent model was adopted including gel microspheres diffusion, which considers the microspheres as homogeneous gel particles where the adsorbed phase diffuses (Ruthven and Loughlin, 1972).

Turner (1958) proposed a model structure where the solid network is described by the branched micro-macropore model, including macropores for the transport and micropores to provide capacity of adsorption or reaction, which was also used later by Villermaux et al. (1987). This model was also applied for the analysis of diffusion and reaction in a catalyst with a bidisperse pore structure (Tartarelli et al., 1970). Recently, the Turner structure of a bidisperse model was adopted to study adsorption, because of its simplicity;

the geometry of macro- and micropores and the diffusivities within pores are then well defined (Petersen, 1991; Silva and Rodrigues, 1999). A similar structure was used to study the competition between diffusion and reaction mechanism and therefore to develop methodologies for the design of reactors using structured catalysts (McGreavy et al., 1994).

The ratio of the diffusion times in the macro- and micropores obtained from adsorption experiments of methanol and isobutylene in gas phase over Amberlyst 15 was found to be of the order of a magnitude of unity. Therefore, in the analysis of rate data for etherification reactions, both macro- and micropore diffusion resistances should be taken into consideration (Oktar et al., 1999). The analysis of the pure component batch adsorption experiments in the liquid phase of ethanol, methanol and 2-methyl-2-butene on Amberlyst 15, using *n*-heptane as inert solvent, has shown that micropore diffusion had insignificant contribution in the total diffusion flux into a macroporous resin catalyst (Dogu et al., 2003). The order of magnitude of the ratio of diffusion times in the macropores and in the gel microspheres is greater than 30 for this system. Therefore a monodisperse pore structure approximation can be made. Moreover, this assumption is supported by the data presented for MTBE synthesis with Amberlyst 15 (Quinta-Ferreira et al., 1996), where the overall efficiency of the catalyst particles was defined by the macroeffectiveness and microeffectiveness factors accounting for the diffusion and reaction processes on the macropores and inside the gel microspheres. The global efficiency of the catalyst was mainly due to the process occurring on the macropores, since the efficiency in the gel microspheres is unity. The mass transfer effects on the kinetics of ETBE synthesis using Amberlyst 15 were modelled by Sundmacher et al. (1995) and his collaborators considering the multicomponent mass transport in the liquid phase of macropores described by the generalized Maxwell–Stefan model, and the transport phenomena through the micropores and the surface diffusion on the gel microspheres were not taken into account explicitly; however, they were lumped in the tortuosity factor. The influence of catalyst particle diameter in the catalytic recovery of anthraquinones was studied in a batch reactor by Wärnå et al. (2002). The authors have used a model that considers the reaction kinetics and intraparticle pore diffusion effects with good agreement with the experimental data. Recently an algorithm for evaluating reactions rates of catalytic reaction networks with strong diffusion limitations was applied to the liquid phase catalytic hydrogenation of butadiene and butyne in butene (Bressa et al., 2001).

In this work, a mathematical model of a batch reactor for heterogeneous catalysis, considering the diffusion of species in the external film and then diffusion through the macropores of the particle and reaction at the microspheres active sites, is developed. The diffusion inside the gel microspheres is considered infinitely fast. Detailed explanations of the numerical solution implemented in the numerical package PDECOL are presented. The model is applied to the analy-

sis of experimental results for diethylacetal synthesis using ethanol and acetaldehyde as reactants and Amberlyst 18 as catalyst. The influence of the mass transfer mechanisms was evaluated by assessing the effectiveness factor values during the transient state of the batch reactor. The effectiveness factor values calculated at equilibrium with the batch reactor model were compared with the values of the effectiveness factor calculated from a steady state infinite bath model.

## 2. Mathematical model of the batch reactor

The model considers that the batch reactor operates in isothermal conditions. The diffusion of species through the external film and then diffusion through the macropores and reaction at the microspheres are also considered.

*Mass balance in the bulk fluid* ( $j = 1, 2, 3$  and 4):

$$\frac{dC_{b,j}}{dt} = -\frac{A_p}{V_{\text{liq}}} D_j \left. \frac{\partial C_{p,j}}{\partial r} \right|_{r=r_p}, \quad (1)$$

$$A_p = \frac{3}{r_p} V_p = \frac{3}{r_p} \frac{1 - \varepsilon_b}{\varepsilon_b} V_{\text{liq}}, \quad (2)$$

where  $C_{b,j}$  is the bulk concentration for species  $j$ ,  $C_{p,j}$  is the concentration of species  $j$  inside the particle,  $A_p$  is the external exchange area between the bulk fluid and the particles,  $V_{\text{liq}}$  is the total volume of reactant mixture,  $D_j$  is the effective diffusivity of species  $j$  inside the pores,  $r_p$  is particle radius,  $V_p$  is the total volume of the particles,  $r$  is the radial position and  $t$  is the time coordinate.

*Mass balance in the intraparticle fluid* ( $j=1, 2, 3$  and 4):

$$\varepsilon_p \frac{\partial C_{p,j}}{\partial t} = \frac{1}{r^2} \frac{\partial}{\partial r} \left[ D_j r^2 \frac{\partial C_{p,j}}{\partial r} \right] + (1 - \varepsilon_p) v_j \rho_{\text{solid}} \mathfrak{R}^p, \quad (3)$$

where  $\varepsilon_p$  is the particle porosity,  $v_j$  is the stoichiometric coefficient of species  $j$ ,  $\rho_{\text{solid}}$  is the true density of the resin and  $\mathfrak{R}^p$  is the reaction rate relative to the local pore concentration.

Initial condition:

$$t = 0, \quad C_{b,j} = C_{b0,j}; \quad C_{p,j} = C_{p0,j}. \quad (4)$$

Boundary conditions:

$$\text{(symmetry condition)} \quad r = 0, \quad \frac{\partial C_{p,j}}{\partial r} = 0, \quad (5)$$

(flow condition)  $r = r_p$ ,

$$D_j \left. \frac{\partial C_{p,j}}{\partial r} \right|_{r=r_p} = k_{f,j} (C_{b,j} - C_{p,j}|_{r=r_p}). \quad (6)$$

Introducing  $\rho = r/r_p$ , the model equations become

$$\frac{dC_{b,j}}{dt} = -\frac{3}{r_p^2} \frac{1 - \varepsilon_b}{\varepsilon_b} D_j \left( \frac{\partial C_{p,j}}{\partial \rho} \right) \Big|_{\rho=1}, \quad (7)$$

where  $\varepsilon_b$  is the bulk porosity.

$$\frac{\partial C_{p,j}}{\partial t} = \frac{D_j}{\varepsilon_p r_p^2} \frac{1}{\rho^2} \frac{\partial}{\partial \rho} \left[ \rho^2 \frac{\partial C_{p,j}}{\partial \rho} \right] + \frac{1 - \varepsilon_p}{\varepsilon_p} v_j \rho_{\text{solid}} \mathfrak{R}^p, \quad (8)$$

$$t = 0, \quad C_{b,j} = C_{b0,j}; \quad C_{p,j} = C_{p0,j}, \quad (9)$$

$$\rho = 0, \quad \frac{\partial C_{p,j}}{\partial \rho} = 0, \quad (10)$$

$$\rho = 1, \quad \left. \frac{\partial C_{p,j}}{\partial \rho} \right|_{\rho=1} = Bi_j (C_{b,j} - C_{p,j} |_{\rho=1}), \quad (11)$$

where  $Bi_j = k_{f,j} r_p / D_j$  is the Biot number for the  $j$  component.

### 3. Numerical solution

The system of partial differential equations (Eqs. (7)–(11)) was solved by the method of lines (MOL) using orthogonal elements, with B-splines as base functions through numerical package PDECOL (Madsen and Sincovec, 1979). This library is specially designed for the solution of the system of PDEs with the structure  $\partial \vec{u} / \partial t = \vec{f}(t, x, \vec{u}, \partial \vec{u} / \partial x, \partial^2 \vec{u} / \partial x^2)$  and it has been used in the simulation of many chemical engineering problems (Lu et al., 1993a,b; Lu and Rodrigues, 1994). For the particular case involved in the mathematical model shown here, the global mass balances for all components, represented by Eq. (7), are ordinary differential equations of first order as a function of  $C_{b,j}$  but coupled with the internal variables of the inside of the particle through the flow conditions for the bulk/intraparticle fluid (see Eq. (11)) and cannot be incorporated in PDECOL when the diffusion in the external film is not negligible (Da Silva, 1998).

(1) *Negligible resistance to external mass transfer* ( $Bi_j \rightarrow \infty$ ). The boundary condition (11) is simplified:

$$\rho = 1, \quad C_{b,j} = C_{p,j} |_{\rho=1}. \quad (12)$$

Additionally, for  $\rho = 1$ , Eq. (8) is replaced by Eqs. (7) and (12). For this particular case, the system of equations obtained can be solved easily with PDECOL, introducing the initial and boundary conditions (9) and (10), respectively, but leaving “free” the boundary condition for  $\rho = 1$ .

(2) *External resistance not negligible*. Eqs. (7) and (8) must be integrated simultaneously. The external liquid volume is perfectly mixed and is in contact with the solid phase (see Fig. 2) and therefore Eq. (7) is replaced by an auxiliary system of equations in partial derivatives defined as

$$\rho = 1, \quad \frac{\partial C_{b,j}}{\partial t} = -\frac{3}{r_p^2} \frac{1 - \varepsilon_b}{\varepsilon_b} D_j \left( \frac{\partial C_{p,j}}{\partial \rho} \right) \Big|_{\rho=1}, \quad (13)$$

$$0 \leq \rho < 1, \quad \frac{\partial C_{b,j}}{\partial t} = 0. \quad (14)$$

Eqs. (13) and (14) have been written with partial derivatives instead of total derivatives as in Eq. (7) in order to recall that

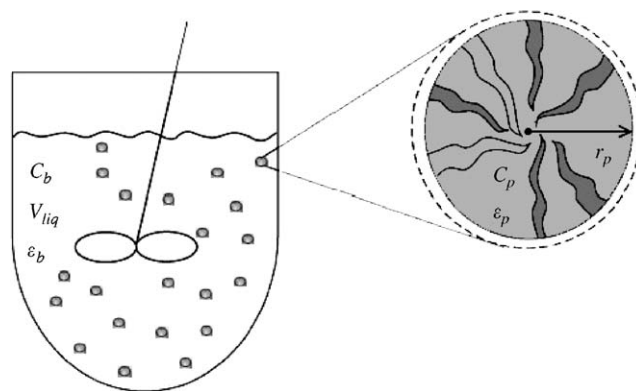


Fig. 2. Schematic figure of the batch reactor model.

now  $C_{b,j}$  are a function of  $t$  and  $\rho$ . Nevertheless, the values of  $C_{b,j}$  inside the beads have no physical meaning with the exception of the values obtained at  $\rho = 1$ , which correspond to the values of the bulk concentration of the batch reactor.

Eqs. (13) and (14) are solved by PDECOL introducing them in the vector  $\vec{f}$  defined as the generic vectorial equation of the system  $\partial \vec{u} / \partial t = \vec{f}(t, x, \vec{u}, \partial \vec{u} / \partial x, \partial^2 \vec{u} / \partial x^2)$  that is required by PDECOL and not through the boundary conditions routine. At the same time, additional boundary conditions at  $\rho = 1$  for the variables  $C_{b,j}$  are not introduced, since the numerical problem becomes fully determined at  $\rho = 1$  with the solution of Eqs. (13) and (14) together with the initial conditions.

At this moment it is important to introduce the following additional observations:

- (a) For  $\rho=0$ , Eq. (8) is not defined and should be substituted by a limiting expression that, using the L'Hopital's rule, is transformed in

$$\frac{\partial C_{p,j}}{\partial t} = \frac{3}{\varepsilon_p r_p^2} D_j \frac{\partial^2 C_{p,j}}{\partial \rho^2} + \frac{1 - \varepsilon_p}{\varepsilon_p} v_j \rho_{\text{solid}} \mathfrak{R}^p. \quad (15)$$

- (b) An important condition for the correct working of PDECOL is the consistency between initial and boundary conditions at time  $t = 0$ . The boundary condition (11) is only compatible “automatically” with the initial conditions (9) if  $C_{b,j}(0) = C_{p,j}(0)$ . However, in the general case, this is not verified, so the compatibility between initial and boundary conditions is achieved by the introduction of the following equation:

$$C_{b,j} - C_{p,j} |_{\rho=1} = \frac{1}{Bi_j} \frac{\partial C_{p,j}}{\partial \rho} \Big|_{\rho=1} + (C_{b0,j} - C_{p0,j}) \exp(-Mt). \quad (16)$$

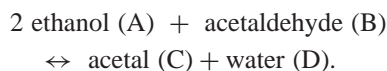
Eq. (16) works as a “switch” allowing to pass from the initial to the required boundary conditions walking through a smooth path, and avoids an abrupt jump or discontinuity that could break the PDECOL starting process. This type of “valve equation” was also used by Lu et al. (1992a,b), where  $M$  is a valve parameter that

must be fixed in order to have a negligible impact in the temporary solution of the process before the starting condition. It can be verified that Eq. (16) is transformed in an identity for  $t = 0$ , since  $\exp(-Mt) = 1$ , changing to the original conditions (see Eq. (11)) for higher values of  $t$ , since  $\exp(-Mt) \rightarrow 0$ .

- (c) For all simulations a tolerance value EPS equal to  $10^{-7}$  was fixed and 20 elements with a uniform spatial grid were used.

#### 4. Results and discussion

For the test of the batch catalytic reactor model and its numerical solution, the synthesis of diethylacetal from ethanol and acetaldehyde catalysed by the ion exchange resin Amberlyst 18 was considered:



The experimental equilibrium and kinetic data were obtained in a batch reactor (Silva and Rodrigues, 2001; Silva, 2003). The experiments to measure the equilibrium constant were carried out in a temperature range 293–333 K. All the experiments lasted long enough for the reaction to reach equilibrium. More details are presented in Appendix A.

Kinetic experiments were performed in the absence of external mass transfer limitations. To quantify the influence of external mass transfer resistance, preliminary experiments at different stirring speed were run. With a stirring speed of 800 rpm, the limitation due to external resistance is eliminated, so all further experiments were done at 800 rpm.

The internal diffusion resistance was evaluated by performing experiments with different particle size. The catalyst was separated by particle size and three classes with different mean diameters were obtained: 267  $\mu\text{m}$  ([180; 354]  $\mu\text{m}$ ), 477  $\mu\text{m}$  ([354; 600]  $\mu\text{m}$ ) and 854  $\mu\text{m}$  ([707; 1000]  $\mu\text{m}$ ). Fig. 3 shows the conversion of acetaldehyde,  $X$ , as a function of time; there are internal diffusion limitations for the experiments with pellet diameters equal to 477 and 854  $\mu\text{m}$ . Relatively to the smaller size of particle, it is not possible to conclude without further studies if mass transfer limitations are absent. Therefore the kinetic experimental data were analysed in order to determine the apparent reaction rate for the pellet with particle diameters of 267  $\mu\text{m}$ .

A two-parameter model based on a Langmuir–Hinshelwood rate expression using activities was proposed to describe the experimental kinetic results, and it was compared with the kinetic rate law expressed in terms of molar fractions. It was assumed that water was the most adsorbed species and therefore just the water adsorption constant appears in the reaction rate equation. This assumption is supported by the adsorption data published for diethylacetal synthesis (Silva and Rodrigues, 2002) and similar systems (Pöpken et al., 2000; Ziyang et al., 2001; Lode et al., 2001) and is different for the one assumed by the authors in a pre-

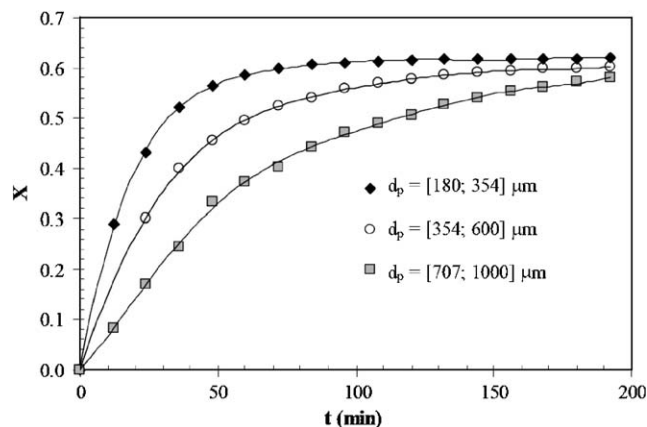


Fig. 3. Effect of catalyst particle size on the conversion of acetaldehyde history:  $T = 288 \text{ K}$ ,  $P = 0.6 \text{ MPa}$ ,  $m_{A0} = 325 \text{ g}$ ,  $r_{A/B} = 2.2$ ,  $w_{\text{cat}} = 1.5 \text{ g}$ ,  $V = 576 \text{ ml}$ .

vious work (Silva and Rodrigues, 2001). Table 2 presents the proposed reaction law in terms of activities and molar fractions and the respective parameters (see Appendix A). The model based on activities provides slightly better agreement between experimental and simulated results.

##### 4.1. Batch catalytic reactor model for negligible external mass transfer resistance

The experimental data were compared with the simulated results using the above apparent reaction rate, where two models were considered. The first one includes the diffusion of the species inside the particle (pore diffusion model), where the diffusivities of the species in the multicomponent liquid mixture are estimated as a function of the local composition by the modified Wilke–Chang equation (Reid et al., 1987). The second considers that the controlling mechanism is the reaction step, so the diffusion inside the particle is infinitely fast (equilibrium model). In this case the concentration inside the pellet macropores is equal to the bulk concentration and Eq. (8) is reduced to

$$\frac{\partial C_{p,j}}{\partial t} = \frac{1 - \varepsilon_p}{\varepsilon_p} v_j \rho_{\text{solid}} \mathfrak{R}, \quad (17)$$

where  $\mathfrak{R}$  is the reaction rate relative to the bulk concentration.

In order to clarify the existence of internal mass transfer resistance in the experiments performed with the smallest pellet diameter, the experimental data were compared with the simulated curves predicted by the equilibrium and pore diffusion models (see Fig. 4). If the internal mass transfer resistance is high, the diffusion flux of the reactants from the bulk to the particle is not sufficiently high to compensate the reaction rate, and therefore there is a concentration profile inside the pellet. This profile decreases the average reaction rate relative to that when the concentration inside the particle is equal to the surface concentration

Table 2  
Kinetic models: reaction law and parameters

	Model in terms of activities	Model in terms of molar fraction
Reaction law	$\mathfrak{R} = k_c \frac{a_A a_B - a_C a_D / K_{eq} a_A}{(1 + K_{s,D} a_D)^2}$	$\mathfrak{R} = k_c \frac{x_A x_B - x_C x_D / K_x x_A}{(1 + K_{s,D} x_D)^2}$
Equilibrium constant (dimensionless)	$K_{eq} = 4.62 \times 10^{-2} \exp\left[\frac{1270.1}{T \text{ (K)}}\right]$	$K_X = 1.50 \times 10^{-2} \exp\left[\frac{1466.5}{T \text{ (K)}}\right]$
Apparent kinetic constant ( $\text{mol g}^{-1} \text{min}^{-1}$ )	$k_c^{\text{app}} = 1.03 \times 10^8 \exp\left[\frac{-5669.9}{T \text{ (K)}}\right]$	$k_c^{\text{app}} = 1.62 \times 10^8 \exp\left[\frac{-5772.0}{T \text{ (K)}}\right]$
Water adsorption constant (dimensionless)	$K_{s,D} = 6.29 \times 10^5 \exp\left[\frac{-3999.3}{T \text{ (K)}}\right]$	$K_{s,D} = 3.42 \times 10^8 \exp\left[\frac{-5803.1}{T \text{ (K)}}\right]$

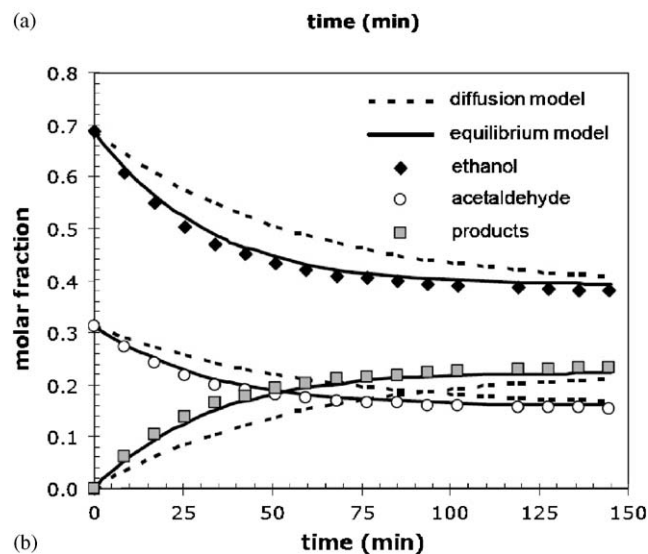
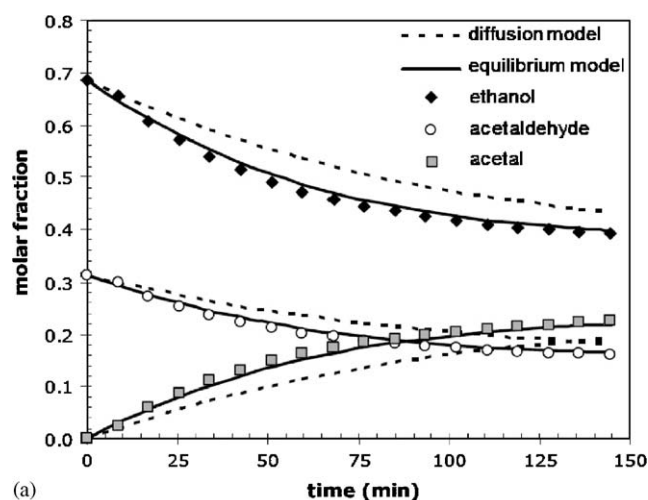


Fig. 4. Comparison between experimental and simulated kinetic curves:  $P = 0.6 \text{ MPa}$ ,  $r_{A/B} = 2.17$ ,  $w_{\text{cat}} = 0.5 \text{ g}$  and  $d_p = 267 \mu\text{m}$ . (a)  $T = 289 \text{ K}$ ; (b)  $T = 299 \text{ K}$ .

(equilibrium model). If the simulated results obtained with the pore diffusion and equilibrium model were identical, the controlling mechanism would be the reaction at the microspheres and therefore the rate equation would be a true reac-

Table 3

Kinetic constant,  $k_c$  ( $\text{mol g}^{-1} \text{min}^{-1}$ ), and the average square errors, SRS, using the kinetic law expressed in terms of activities and molar fractions

$T$ (K)	Model (activities)		Model (molar fraction)	
	$k_c$	SRS	$k_c$	SRS
289	0.605	$2.9 \times 10^{-5}$	0.683	$3.8 \times 10^{-5}$
293	0.807	$2.7 \times 10^{-5}$	1.942	$3.2 \times 10^{-5}$
299	1.481	$3.7 \times 10^{-5}$	1.750	$4.2 \times 10^{-5}$

tion rate. According to this and from the comparison between pore diffusion and equilibrium models results shown in Fig. 4, it is possible to conclude that the measured kinetic results were masked by intraparticle mass transfer limitations.

In order to determine the true kinetic constant, an optimization of the kinetic data was performed. The estimation of the kinetic constant was carried out with a non-linear regression subroutine that uses the Levenberg–Marquardt method to minimise the sum of residual squares (SRS) between the experimental and calculated molar fraction of all components:

$$\text{SRS} = \sum_{i=1}^4 \sum_{j=1}^n (x_{i,\text{exp}} - x_{i,\text{theo}})^2. \quad (18)$$

The theoretical molar fractions ( $x_{i,\text{theo}}$ ) were calculated by the proposed model, in the absence of external mass transfer. The values of the true kinetic constant for the models expressed in terms of activities and molar fractions are presented in Table 3.

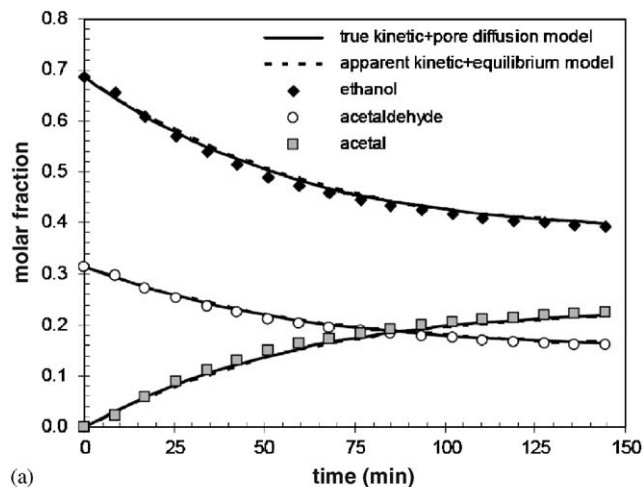
The kinetic model expressed in terms of activities is slightly more accurate than the model expressed in terms of molar fractions. But the last one is simpler and also provides good results. The temperature dependence of kinetic constants was fitted with the Arrhenius equation, leading to:

$$\text{activities: } k_{0,c} = 3.32 \times 10^{11} \text{ mol g}^{-1} \text{min}^{-1};$$

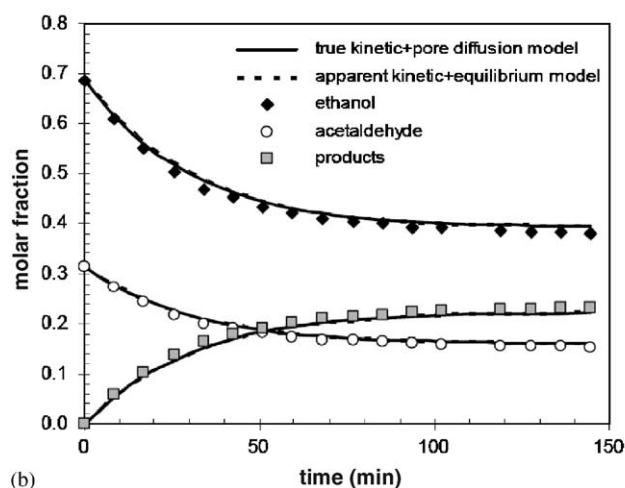
$$E_{a,c} = 65.1 \text{ kJ mol}^{-1};$$

$$\text{molar fractions: } k_{0,c} = 1.40 \times 10^{12} \text{ mol g}^{-1} \text{min}^{-1};$$

$$E_{a,c} = 6.82 \text{ kJ mol}^{-1}.$$



(a)



(b)

Fig. 5. Comparison between experimental points and optimized kinetic curves (apparent kinetic+equilibrium model and true kinetic+pore diffusion model):  $P = 0.6$  MPa,  $r_{A/B} = 2.18$ ,  $w_{\text{cat}} = 0.5$  g and  $d_p = 267$   $\mu\text{m}$ . (a)  $T = 289$  K; (b)  $T = 299$  K.

The comparison between the experimental values and the theoretical models (apparent kinetic+equilibrium model and true kinetic+pore diffusion model), for all temperatures and stoichiometric initial composition of reactants, is shown in Fig. 5.

The experimental and simulated values of the molar fraction of ethanol and acetal as a function of time, for experiments using catalyst pellets with 267, 477 and 854  $\mu\text{m}$  diameter, are shown in Fig. 6. The agreement between the experimental data and the results simulated with the pore diffusion model leads us to conclude that the mass transfer parameters are well predicted by the correlations mentioned above.

#### 4.2. Intraparticle concentration profiles and effectiveness factor

Fig. 7 shows the internal concentration profiles accessed by simulations at two different times. It is possible to con-

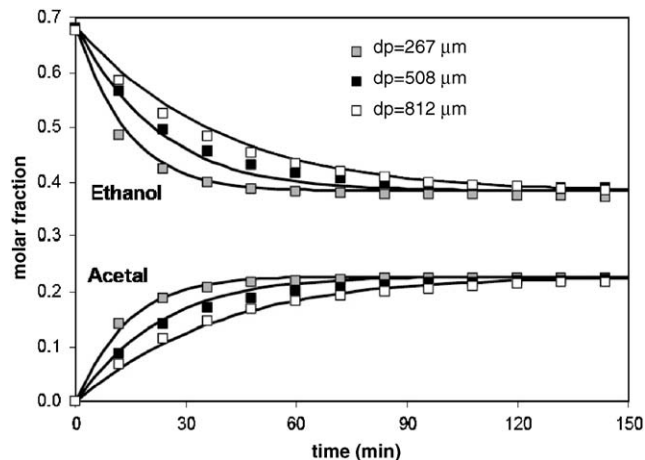
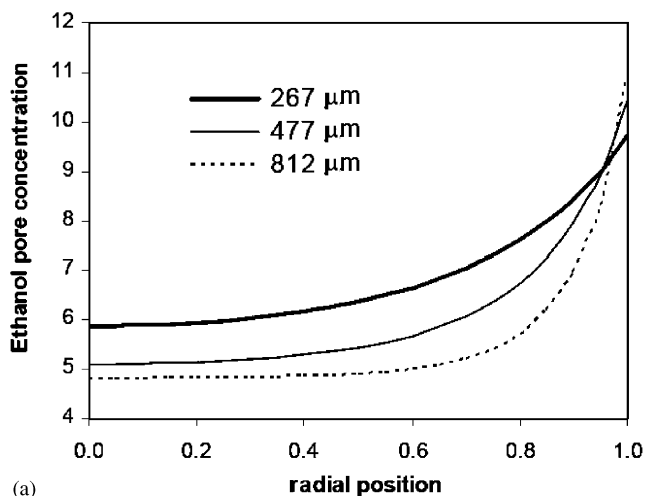
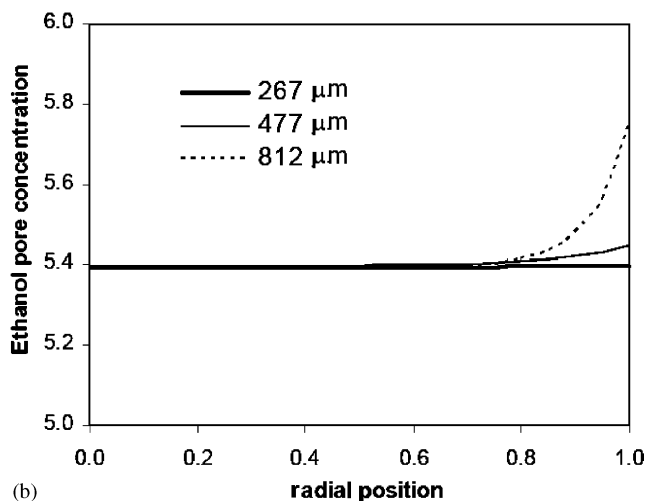


Fig. 6. Effect of catalyst particle diameter on the molar fraction of ethanol and acetal as a function of time:  $T = 293$  K,  $r_{A/B} = 2.17$ ,  $P = 0.6$  MPa and  $w_{\text{cat}} = 1.5$  g. Points are experimental data, lines are simulated results.



(a)



(b)

Fig. 7. Effect of catalyst particle diameter on the internal concentration profile of ethanol ( $\text{mol dm}^{-3}$ ), experimental conditions of Fig. 6. (a)  $t = 5$  min; (b)  $t = 100$  min.

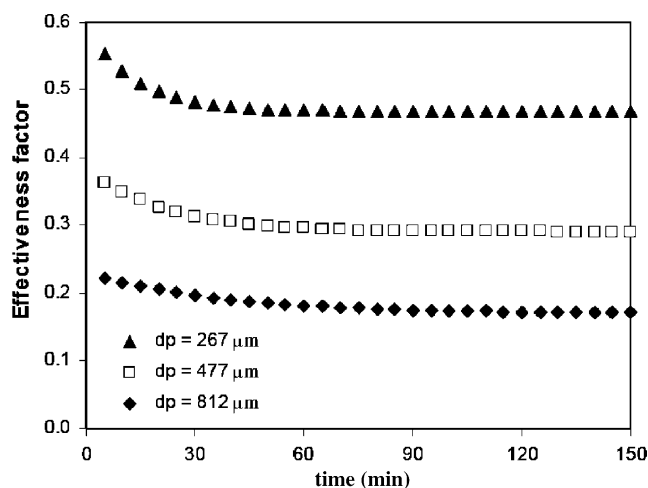


Fig. 8. Effect of catalyst particle diameter on the effectiveness factor history.

clude that pore diffusion is the controlling mechanism because of the concentration gradient between the surface and the centre of a catalyst particle. The effectiveness factor could be evaluated at each time by knowing the concentration inside the particle.

The effectiveness factor is defined as

$$\eta = \frac{\langle \mathfrak{R} \rangle}{\mathfrak{R}_s} = 3 \frac{\int_0^1 \rho^2 \mathfrak{R} d\rho}{\mathfrak{R}_s} \quad (19)$$

where  $\mathfrak{R}_s$  is the kinetic rate at surface conditions and  $\langle \mathfrak{R} \rangle$  is the average kinetic rate defined as

$$\langle \mathfrak{R} \rangle = \frac{\int_0^{r_p} r^2 \mathfrak{R} dr}{\int_0^{r_p} r^2 dr} \quad (20)$$

The time evolution of the effectiveness factor, for different particle diameter, is represented in Fig. 8.

It is interesting to note that when equilibrium is reached, the rates of the direct and the reverse reactions are equal, meaning that reaction rate  $\mathfrak{R}$  is zero, both at the surface and inside the particle.

This should imply that the effectiveness factor was not defined:  $\eta_\infty = \lim_{t \rightarrow \infty} (\langle \mathfrak{R} \rangle / \mathfrak{R}_s) = 0/0$ .

In order to clarify the meaning of the value obtained by numerical integration, the values of the effectiveness factor for the same experiments were calculated assuming an infinite bath where the surface concentration is equal to the initial bulk concentration of the batch reactor. The steady state profiles obtained in an infinite bath are shown in Fig. 9. The corresponding effectiveness factors are presented in Table 4. The steady state values of effectiveness factors obtained from the infinite bath model are higher than those obtained from the batch reactor.

For better understanding, a slab of porous catalyst where a first-order reversible chemical reaction ( $A \rightleftharpoons B$ ) takes place

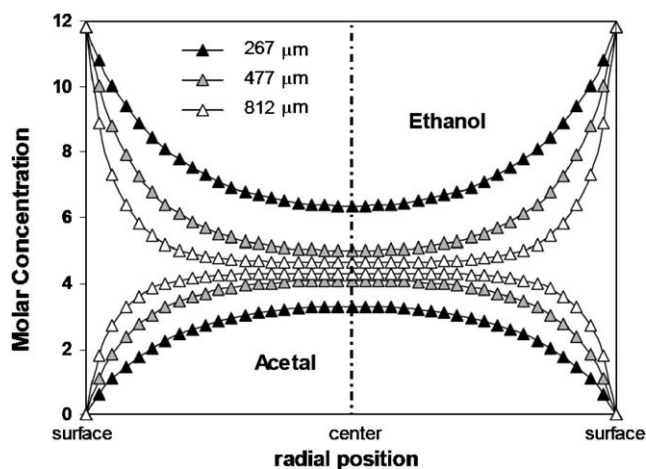


Fig. 9. Effect of catalyst particle diameter on the ethanol and acetal internal concentration profiles at steady state, for an infinite bath:  $C_{A,s} = 11.8 \text{ mol dm}^{-3}$ ,  $C_{B,s} = 5.5 \text{ mol dm}^{-3}$ ,  $T = 293 \text{ K}$ ,  $P = 0.6 \text{ MPa}$ .

Table 4

Comparison of the effectiveness factors obtained for the batch reactor (BR) and the infinite bath (IB), at steady state, for different particle diameters:  $T = 293 \text{ K}$ ,  $r_{A/B} = 2.17$ ,  $P = 0.6 \text{ MPa}$  and  $w_{\text{cat}} = 1.5 \text{ g}$

$d_p$ ( $\mu\text{m}$ )	Effectiveness factor	
	BR	IB
267	0.469	0.558
477	0.291	0.365
812	0.172	0.222

is studied in Appendix B. The main conclusions are:

- The effectiveness factor, for an infinite bath and for a first-order reaction of type  $A \rightleftharpoons B$ , is independent of the surface composition.
- The effectiveness factor for the batch reactor, assuming that at each time there is a pseudo-steady-state internal profile corresponding to the pellet surface composition (by making the time derivative of the pore concentration equal to zero), is equal to the value obtained in the infinite bath.

For the acetal synthesis it is not possible to reach the same conclusions, since all properties (total molar concentration and viscosity of the mixture, activities and diffusivities of the species) are being estimated instantaneously and locally. Since the surface concentration is constant in the infinite bath and is varying with time in the batch reactor, the internal concentration profiles at the steady state for both situations are different (see Table 5), leading to deviations in the values of the effectiveness factors. The effectiveness factor calculated with the batch reactor model at a certain time is equal to the one calculated with the infinite bath model using as surface concentration the bulk concentration of the batch reactor at that time, meaning that the transient evaluation of the

Table 5

Composition and viscosity of the mixture and molecular diffusivity of the species evaluated at the surface of the particle, for the batch reactor (BR) and the infinite bath (IB) at steady state

	Concentration (mol dm <sup>-3</sup> )			Viscosity (mPa s)	Molecular diffusivity (cm <sup>2</sup> min <sup>-1</sup> )			
	Ethanol	Acetaldehyde	Products		Ethanol	Acetaldehyde	Acetal	Water
IB	11.83	5.46	0.00	0.653	1.4 × 10 <sup>-3</sup>	1.4 × 10 <sup>-3</sup>	8.0 × 10 <sup>-4</sup>	2.7 × 10 <sup>-3</sup>
BR	5.39	2.24	3.22	0.778	1.2 × 10 <sup>-3</sup>	1.2 × 10 <sup>-3</sup>	7.1 × 10 <sup>-4</sup>	2.5 × 10 <sup>-3</sup>

Table 6

Effectiveness factors evaluation for the infinite bath: concentration and molecular diffusivity of the species evaluated at the surface of the particle

T (°C)	Concentration (mol dm <sup>-3</sup> )			k <sub>c</sub> (mol g <sup>-1</sup> min <sup>-1</sup> )	Molecular diffusivity (cm <sup>2</sup> min <sup>-1</sup> )			
	Ethanol	Acetaldehyde	Products		Ethanol	Acetaldehyde	Acetal	Water
10	12.01	5.54	0.00	0.33	1.1 × 10 <sup>-3</sup>	1.1 × 10 <sup>-3</sup>	6.5 × 10 <sup>-4</sup>	2.3 × 10 <sup>-3</sup>
20	11.83	5.46	0.00	0.85	1.4 × 10 <sup>-3</sup>	1.4 × 10 <sup>-3</sup>	8.0 × 10 <sup>-4</sup>	2.7 × 10 <sup>-3</sup>

effectiveness factor could be obtained using the pseudo-steady-state model. This is supported by the fact that the diffusion time needed to get a concentration profile inside the particle at 99% of the concentration step at the external surface is  $t_F = 0.39r_p^2/(D_{m,j}/\tau)$  and is much lower than the reaction time. The diffusion time can be estimated from Carslaw and Jaeger (1959) as  $t_F = 1.8$  min, considering the biggest particle used ( $d_p = 0.0812$  cm) and the species with the lowest molecular diffusivity ( $D_{m,acetal} = 7.1 \times 10^{-4}$  cm<sup>2</sup> min<sup>-1</sup>). According to Fig. 7(c), the reaction time needed to reach 99% of equilibrium composition is about 150 min, two orders of magnitude higher than  $t_F$ . This result suggests that for this system the transient effects inside the particles could be neglected and a pseudo-steady-state model is applicable.

In order to identify the controlling mechanism, the Thiele modulus was defined at the surface conditions:

$$\phi_A = \frac{r_p}{3} \sqrt{\frac{\rho_p k_c}{D_{A_s} C_{A_s}}}, \quad (21)$$

where  $r_p$  is the particle radius,  $\rho_p$  is the particle density,  $k_c$  is the kinetic constant,  $D_{A_s}$  is the effective diffusivity of ethanol at the surface and  $C_{A_s}$  is the ethanol concentration at the surface. For values greater than unity, the internal diffusion is the limiting step. The variation of the effectiveness factor with the Thiele modulus and the temperature was evaluated by using the infinite bath model. The values of molar concentrations and molecular diffusivities of the species calculated at the surface are presented in Table 6. In the above calculations particle density  $\rho_p = 1205$  g/dm<sup>3</sup>, internal porosity  $\varepsilon_p = 0.48$  and tortuosity  $\tau = 2$  were assumed. Graphical representation of the effectiveness factor versus the Thiele modulus is available as Fig. 10.

The temperature will affect all properties estimation, but the effect on effectiveness factor dependence on Thiele modulus is small.

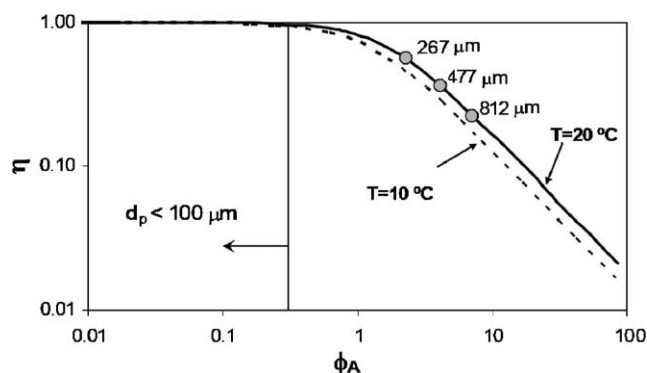


Fig. 10. Variation of the effectiveness factor with Thiele modulus and temperature.

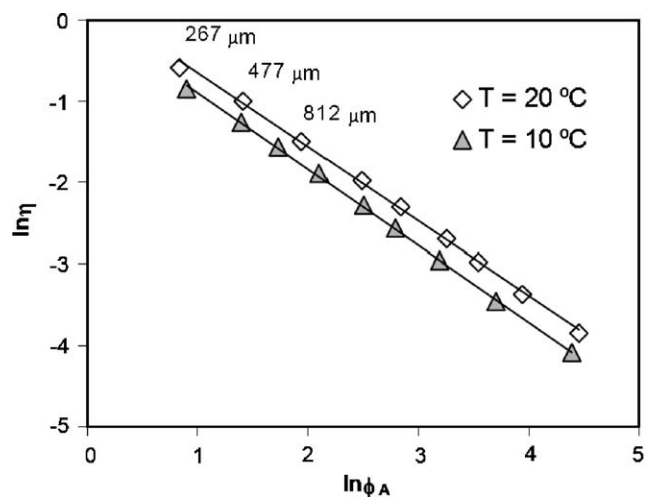


Fig. 11. Dependence of the effectiveness factor on Thiele modulus.

The relation between the effectiveness factor and the Thiele modulus (see Fig. 11), when the internal diffusion is

the controlling mechanism, is given by:

$$T = 283 \text{ K: } \ln \eta = -0.936 \ln \phi_A + 0.036;$$

$$T = 29 \text{ K: } \ln \eta = -0.913 \ln \phi_A + 0.250.$$

## 5. Conclusions

A model of the batch reactor for heterogeneous catalysis considering the diffusion of the species in the external film and then diffusion through the macropores of the particle and reaction at the microspheres sites was developed. The reaction process was considered to be isothermal.

The numerical solution was obtained through a clever use of the package PDECOL. Simulations have shown that the effectiveness factor varies during the transient state of the batch reactor but tends to an equilibrium value. The values obtained by numerical integration were compared with those calculated from a steady state infinite bath model. The steady state values of effectiveness factors obtained from the infinite bath model are higher than those obtained from the batch reactor. The explanation for such a difference is that the internal concentration profile at a certain time is not in equilibrium with the surface concentration, for the batch reactor during the transient state. This is supported by the fact that the effectiveness factor for the batch reactor, assuming a pseudo-steady-state (at each time the internal profiles are in equilibrium with the surface composition by making the time derivative of the particle concentration, zero), is equal to the value obtained in the infinite bath.

The model was applied to the diethylacetal synthesis using ethanol and acetaldehyde as reactants and Amberlyst 18 as catalyst. The simulated results have shown that kinetic experiments performed with the smaller particle size of catalyst were masked by mass transfer limitations. The experimental data were fitted in order to get the true kinetic constant.

## Notation

$a$	liquid phase activity
$A_p$	external exchange area between the bulk fluid and the particles
$Bi$	Biot number
$C_i$	concentration, $\text{mol dm}^{-3}$
$C_b$	bulk concentration, $\text{mol dm}^{-3}$
$C_p$	concentration inside the particle, $\text{mol dm}^{-3}$
$d_p$	average pellet diameter, $\mu\text{m}$
$D_j$	effective diffusivity of species $j$ inside the pores, $\text{cm}^2 \text{min}^{-1}$
$E_{a,c}$	reaction activation energy, $\text{J mol}^{-1}$
$k_c$	kinetic constant, $\text{mol g}^{-1} \text{min}^{-1}$
$k_{0,c}$	Arrhenius constant, $\text{mol g}^{-1} \text{min}^{-1}$
$k_f$	external film coefficient, $\text{cm min}^{-1}$
$K_{\text{eq}}$	equilibrium reaction constant based on activities
$K_x$	equilibrium constant based on molar fractions
$K_\gamma$	equilibrium constant based on activity coefficients

$K_s$	equilibrium adsorption constant
$m$	mass, g
$n$	number of moles, mol
$P$	pressure, Pa
$r$	radial position, cm
$r_p$	particle radius, $\mu\text{m}$
$r_{A/B}$	initial molar ratio of reactants
$\mathfrak{R}$	reaction rate, $\text{mol g}^{-1} \text{min}^{-1}$
$\mathfrak{R}_s$	reaction rate at surface conditions, $\text{mol g}^{-1} \text{min}^{-1}$
$\langle \mathfrak{R} \rangle$	average reaction rate, $\text{mol g}^{-1} \text{min}^{-1}$
$\mathfrak{R}^p$	reaction rate relative to the local pore concentration, $\text{mol g}^{-1} \text{min}^{-1}$
$t$	time coordinate, min
$T$	temperature, K
$x$	molar fraction
$X$	conversion of the limiting reactant
$V$	volume of solution, $\text{cm}^{-3}$
$V_{\text{liq}}$	total volume of reactant mixture, $\text{cm}^3$
$V_p$	total volume of the particles, $\text{cm}^3$
$w_{\text{cat}}$	mass of dry catalyst, g

## Greek letters

$\gamma$	activity coefficient
$\varepsilon_b$	bulk porosity
$\varepsilon_p$	particle porosity
$\eta$	effectiveness factor
$\nu$	stoichiometric coefficient
$\rho$	dimensionless radial coordinate
$\rho_p$	particle density, $\text{g dm}^{-3}$
$\rho_{\text{solid}}$	true density of the resin, $\text{g dm}^{-3}$
$\phi$	Thiele modulus

## Subscripts

$A$	ethanol
$B$	acetaldehyde
$C$	acetal
$D$	water
$e$	equilibrium
$i$	relative to component $i$
liq	liquid phase
$s$	relative to the surface of the particle

## Acknowledgements

We gratefully acknowledge the financial support of FCT—Fundação para a Ciência e Tecnologia, project Grant POCTI/EQU/40695/2001.

## Appendix A. Preliminary kinetic studies in a batch reactor

### A.1. Equilibrium constant determination

The experiments to measure the equilibrium constant were carried out in a temperature range 283–333 K, at 1.0 MPa,

Table A.1  
Experimental equilibrium composition expressed in molar fraction

<i>T</i> (°C)	Acetaldehyde	Ethanol	Acetal	Water
20	0.1583	0.3862	0.2278	0.2278
30	0.1648	0.3930	0.2211	0.2211
40	0.1699	0.4029	0.2136	0.2136
60	0.1806	0.4234	0.1980	0.1980

Table A.2  
Relative molecular volume and surface area of pure species parameters (Reid et al., 1987)

Molecule (i)	Group identification			$v_k^{(i)}$	$R_k$	$Q_k$
	Name	No. main	No. sec.			
1-ethanol	CH <sub>3</sub>	1	1	1	0.9011	0.848
	CH <sub>2</sub>	1	2	1	0.6744	0.540
	OH	5	15	1	1.0000	1.200
2-acetaldehyde	CH <sub>3</sub>	1	1	1	0.9011	0.848
	CHO	10	21	1	0.9980	0.948
3-acetal	CH <sub>3</sub>	1	1	3	0.9011	0.848
	CH	1	3	1	0.4469	0.228
	CH <sub>2</sub> O	13	26	2	0.9183	0.780
4-water	H <sub>2</sub> O	7	17	1	0.9200	1.400

with 1.5 g of dry catalyst, reaction volume of 600 cm<sup>3</sup>, and initial molar ratio of reactants  $r_{A/B}=2.2$ . All the experiments lasted long enough for the reaction to reach equilibrium. Table A.1 shows the experimental conditions and the average equilibrium composition at each temperature.

The thermodynamic equilibrium constant for the liquid phase reaction considered as a non-ideal system is given by

$$K_{\text{eq}} = \frac{a_{C_e} a_{D_e}}{a_{A_e}^2 a_{B_e}} = \frac{x_{C_e} x_{D_e} \gamma_C \gamma_D}{x_{A_e}^2 x_{B_e} \gamma_A^2 \gamma_B} = K_x K_\gamma \quad (\text{A.1})$$

The equilibrium constant was also evaluated in terms of molar fractions, if the mixture has an ideal behaviour:

$$K_x = \frac{x_{C_e} x_{D_e}}{x_{A_e}^2 x_{B_e}} \quad (\text{A.2})$$

The activity coefficients of compounds were computed by the UNIFAC method (Fredeslund et al., 1977). The parameters relative molecular volume and surface area of pure species and the interaction parameters used in this work are presented in Tables A.2 and A.3. The activity coefficients obtained are shown in Table A.4.

The equilibrium constants calculated in terms of molar fraction and activities are presented in Table A.5.

#### A.2. Parameter estimation from kinetic experimental data

The kinetic experiments were carried out in a temperature range 288–299 K, at 0.6 MPa, with 0.5 g of dry catalyst with

Table A.3  
Interaction parameters (Fredeslund et al., 1998)

$a_{m,n}$	1	5	7	10	13
1	0	986.5	1318	677	251.5
5	156.4	0	353.5	−203.6	28.06
7	300	−229.1	0	−116	540.5
10	505.7	529	480.8	0	304.1
13	83.36	237.7	−314.7	−7.838	0

Table A.4  
Activity coefficients for the equilibrium composition

<i>T</i> (K)	Ethanol	Acetaldehyde	Acetal	Water
293	1.072	1.194	1.365	1.587
303	1.077	1.196	1.369	1.630
313	1.082	1.197	1.374	1.668
333	1.086	1.196	1.385	1.742

Table A.5  
Equilibrium constants determined from experimental data

<i>T</i> (K)	$K_x$	$K_a$
293	2.198	3.472
303	1.921	3.086
313	1.655	2.708
333	1.211	2.072

267 μm of particle diameter, reaction volume of 600 cm<sup>3</sup> and values of initial molar ratio of reactants equal to 1.47, 2.17 and 3.34.

A model based on a Langmuir–Hinshelwood rate expression using activities was proposed to describe the experimental kinetic results:

$$\mathfrak{R} = k_c \frac{a_A a_B - a_C a_D / K_{\text{eq}} - a_A}{(1 + K_{s,C} a_C)^2} \quad (\text{A.3})$$

In order to reduce the number of optimization parameters a rate equation was derived from Eq. (A.3) by assuming that water is more adsorbed than the other species. The simplified rate equation is then

$$\mathfrak{R} = k_c \frac{a_A a_B - a_C a_D / K_{\text{eq}} a_A}{(1 + K_{s,D} a_D)^2} \quad (\text{A.4})$$

The kinetic model contains two parameters: the kinetic constant ( $k_c$ ) and the water adsorption parameter ( $K_{s,D}$ ).

The mass balance in a batch reactor for acetal, in the liquid phase, at constant temperature and assuming that intra-particle mass transfer is negligible, is

$$\frac{dn_C}{dt} = w_{\text{cat}} \mathfrak{R} \quad (\text{A.5})$$

Table A.6

Kinetic constant,  $k_c$  ( $\text{mol g}^{-1} \text{min}^{-1}$ ), water adsorption constant,  $K_{s,D}$  (dimensionless), and average square errors, RS, using the kinetic law expressed in terms of activities and molar fractions

$T$ (K)	Model in terms of activities			Model in terms of molar fractions		
	$k_c$	$K_{s,C}$	RS	$k_c$	$K_{s,D}$	RS
289	0.321	0.631	$1.9 \times 10^{-5}$	0.356	0.675	$2.2 \times 10^{-5}$
293	0.395	0.724	$1.8 \times 10^{-5}$	0.440	0.824	$2.0 \times 10^{-5}$
299	0.614	0.996	$5.0 \times 10^{-5}$	0.689	1.309	$5.4 \times 10^{-5}$

Table A.7

Arrhenius parameters for the kinetic and adsorption constant

Model	$k_{0,c}$ ( $\text{mol g}^{-1} \text{min}^{-1}$ )	$E_{a,c}$ ( $\text{kJ mol}^{-1}$ )	$K_{0,sD}$ (—)	$\Delta H_{s,D}$ ( $\text{kJ mol}^{-1}$ )
Activities	$1.03 \times 10^8$	47.1	$6.29 \times 10^5$	33.3
Molar fraction	$1.63 \times 10^8$	48.0	$3.42 \times 10^8$	48.2

where  $n_c$  is the number of moles of acetal,  $t$  is the time,  $w_{\text{cat}}$  is the mass of catalyst and  $\mathfrak{R}$  is the reaction rate referred to the catalyst mass.

The suggested reaction rate was fitted, at each temperature, to the experimentally measured rates of reaction. The estimation of model parameters was carried out with a non-linear regression subroutine *dr8lin* (IMSL, 1991) that uses the Levenberg–Marquardt method to minimise the sum of residual squares (SRS) between the experimental and calculated rate of reaction:

$$\text{SRS} = \sum (\mathfrak{R}_{\text{exp}} - \mathfrak{R}_{\text{theo}})^2. \quad (\text{A.6})$$

The kinetic rate law expressed in terms of activities was compared with the kinetic rate law expressed in terms of molar fractions. The values of the optimized parameters for each model are presented in Table A.6. The model based on molar fraction provides also a good fitting; however, the error is slightly higher than when activities are used.

The temperature dependence of kinetic and water adsorption constants were fitted with the Arrhenius equation, leading to the parameters presented in Table A.7.

## Appendix B. Effectiveness factor of a slab catalyst for reversible reaction $A \rightleftharpoons B$

In order to understand the concept of effectiveness factor in a batch reactor when the equilibrium is achieved, the case of a slab porous catalyst where a first-order reversible chemical reaction ( $A \rightleftharpoons B$ ) takes place is studied. This is an extension of the work of Paiva and Malcata (1997).

### B.1. Effectiveness factor in an infinite bath

Let us consider a slab porous catalyst, as shown in Fig. B.1. Assuming a first-order reversible chemical reac-

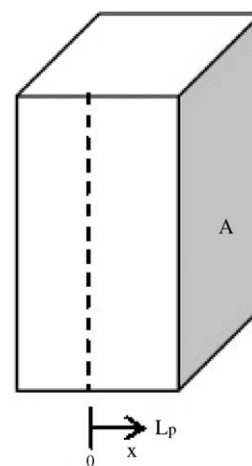


Fig. B.1. Schematic representation of a slab porous catalyst.

tion ( $A \rightleftharpoons B$ ), the mass balance equations for an infinite bath at steady state are

$$D_A \frac{d^2 C_A}{dx^2} - (k_A C_A - k_B C_B) = 0, \quad (\text{B.1})$$

$$D_B \frac{d^2 C_B}{dx^2} + (k_A C_A - k_B C_B) = 0 \quad (\text{B.2})$$

with the boundary conditions ( $i = A, B$ )

$$x = 0, \quad \frac{dC_i}{dx} = 0, \quad (\text{B.3})$$

$$x = L_p, \quad C_i = C_{i,s}. \quad (\text{B.4})$$

Since in the steady state the sum of the diffusional fluxes of all species is zero, the mass balance to product B may be

Table B.1  
Infinite bath model parameters

$L_p = 1 \times 10^{-3} \text{ m}$
$D_A = 2 \times 10^{-8} \text{ m}^2 \text{ s}^{-1}$
$D_B = 1 \times 10^{-8} \text{ m}^2 \text{ s}^{-1}$
$k_A = 0.02 \text{ s}^{-1}$
$k_B = 0.2 \text{ s}^{-1}$
$K_{\text{eq}} = 0.1$
$\alpha^2 = 21$
$\gamma = 2$
$\phi = 1$

written as

$$D_A \frac{dC_A}{dx} + D_B \frac{dC_B}{dx} = 0. \quad (\text{B.5})$$

Integration of Eq. (B.5) using the stated boundary conditions yields

$$C_B = C_{B,s} + \frac{D_A}{D_B} (C_{A,s} - C_A). \quad (\text{B.6})$$

The analytical solution for the internal concentration profile is (for all  $C_{A,0}$  and  $C_{B,0}$ ):

$$\frac{C_A}{C_{A,s}} = \frac{K_{\text{eq}} - r_s \cosh(\alpha x/L_p)}{K_{\text{eq}} + \gamma \cosh(\alpha)} + \frac{r_s + \gamma}{K_{\text{eq}} + \gamma}, \quad (\text{B.7})$$

where

$$\text{equilibrium constant: } K_{\text{eq}} = k_A/k_B, \quad (\text{B.8})$$

$$\text{diffusivities ratio: } \gamma = D_A/D_B, \quad (\text{B.9})$$

$$\text{surface concentrations ratio: } r_s = C_{B,s}/C_{A,s}. \quad (\text{B.10})$$

$$\text{Thiele modulus: } \phi = L_p \sqrt{\frac{k_A}{D_A}}. \quad (\text{B.11})$$

$$\text{modified Thiele modulus: } \alpha = \phi \sqrt{1 + \gamma/K_{\text{eq}}}. \quad (\text{B.12})$$

Define the effectiveness factor as

$$\eta = \frac{\int_{-L}^{+L} A[k_A C_A(x) - k_B C_B(x)] dx}{2AL(k_A C_{A,s} - k_B C_{B,s})}. \quad (\text{B.13})$$

After integration and algebraic rearrangement it becomes

$$\eta = \frac{\tanh(\alpha)}{\alpha}, \quad (\text{B.14})$$

which is independent of the surface concentration.

As an example, let us consider the parameter values presented in Table B.1; the effectiveness factor obtained is  $\eta = 0.218$ .

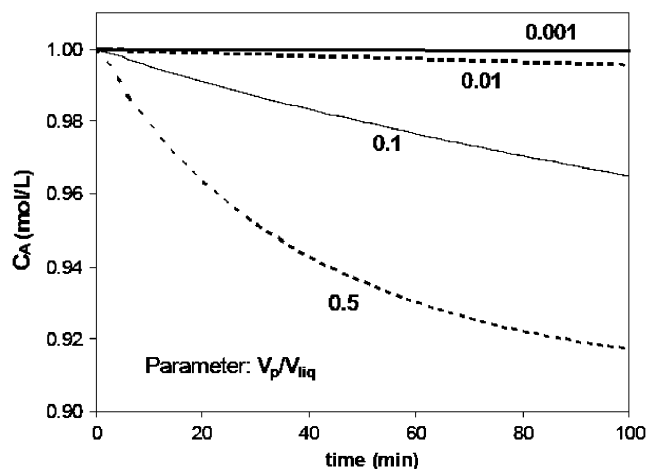


Fig. B.2. Effect of the parameter  $V_p/V_{\text{liq}}$  in the bulk concentration profile of the reactant.

## B.2. Effectiveness factor in a batch reactor

The mass balance equations in a batch reactor for a transient state are:

- for the bulk:

$$\frac{\partial C_{b,A}}{\partial t} = -\frac{A_p}{V_{\text{liq}}} D_A \frac{\partial C_A}{\partial x} \Big|_{x=L_p}, \quad (\text{B.15})$$

$$\frac{\partial C_{b,B}}{\partial t} = -\frac{A_p}{V_{\text{liq}}} D_B \frac{\partial C_B}{\partial x} \Big|_{x=L_p}, \quad (\text{B.16})$$

$$\frac{A_p}{V_{\text{liq}}} = \frac{1}{L_p} \frac{V_p}{V_{\text{liq}}}; \quad (\text{B.17})$$

- inside the particle:

$$\varepsilon_p \frac{\partial C_A}{\partial t} = D_A \frac{\partial^2 C_A}{\partial x^2} - (k_A C_A - k_B C_B), \quad (\text{B.18})$$

$$\varepsilon_p \frac{\partial C_B}{\partial t} = D_B \frac{\partial^2 C_B}{\partial x^2} + (k_A C_A - k_B C_B) \quad (\text{B.19})$$

with the boundary conditions ( $i = A, B$ )

$$x = 0, \quad \frac{dC_i}{dx} = 0, \quad (\text{B.20})$$

$$x = L_p, \quad C_i = C_{b,i} \quad (\text{B.21})$$

and initial conditions ( $i = A, B$ )

$$t = 0, \quad C_i = 0, \quad C_{b,i} = C_{i,s}. \quad (\text{B.22})$$

For the values used in the example before, the effect of  $V_p/V_{\text{liq}}$  ( $\varepsilon_p = 0.4$ ) on bulk concentration is shown in Fig. B.2.

For small values of  $V_p/V_{\text{liq}}$  the bulk composition almost does not change with time (infinite bath) and the effectiveness factor tends to the value determined by the infinite bath, as shown in Table B.2.

Table B.2  
Effect of the parameter  $V_p/V_{liq}$  in the bulk concentration profiles

$V_p/V_{liq}$	$\eta$
0.5	0.222
0.1	0.219
0.01	0.218
0.001	0.218
Infinite bath	0.218

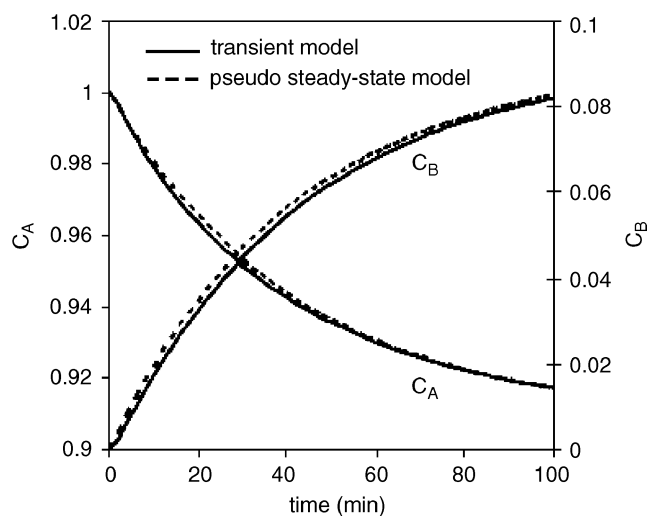


Fig. B.3. Bulk concentration profiles: comparison between the transient and pseudo-steady-state models:  $V_p/V_{liq} = 0.5$ .

From the results obtained from the infinite bath model, where the effectiveness factor does not change with the external (surface) composition, it was reasonable to expect the same effectiveness factor for the batch reactor. However, Table B.2 shows that the effectiveness factor for finite bath (batch reactor) is different from that obtained with infinite bath. The explanation for such a difference is that the internal concentration profile at a certain time is not in equilibrium with the surface concentration.

The internal concentration profiles were calculated from a complete batch reactor model and from a pseudo-steady-state batch reactor model (the time derivative in Eq. (B.18) is zero), where the internal concentration profile is at each moment in equilibrium with the surface concentration. Fig. B.3 shows the bulk concentration history from the transient and the pseudo-steady-state models. The effectiveness factors obtained were 0.222 and 0.218, respectively. The internal concentration profiles, at various times, are shown in Fig. B.4. It is possible to conclude that:

- the effectiveness factor is independent of the surface composition, if the internal concentration profile is in equilibrium with the surface concentration;
- the effectiveness factor for the batch reactor, assuming a pseudo-steady-state (at each time the internal profiles are in equilibrium with the surface composition), is equal to the value obtained in the infinite bath.

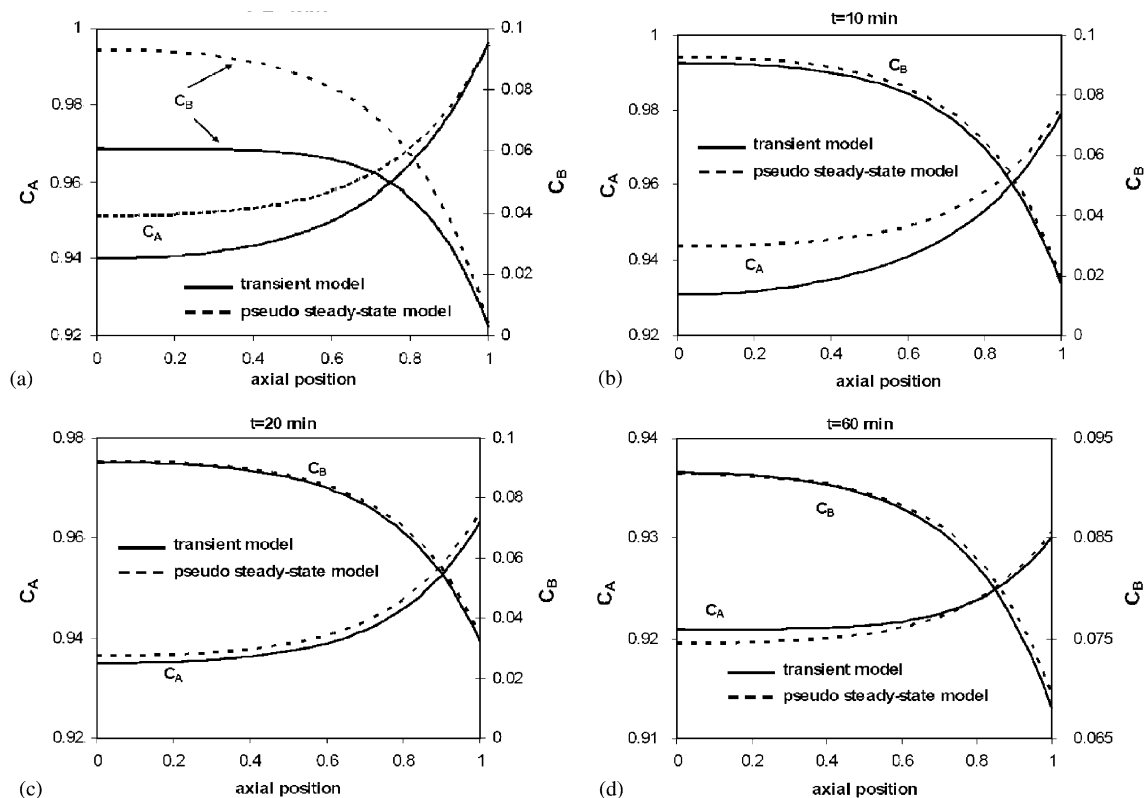


Fig. B.4. Internal concentration profiles: comparison between the transient and pseudo-steady-state models: (a)  $t = 2$  min; (b)  $t = 10$  min; (c)  $t = 20$  min; (d)  $t = 60$  min.

## References

- Ali, A., Bhatia, S., 1990. Methyl tertiary butyl ether formation in a catalytic bed reactor—kinetic and modelling study. *Chemical Engineering Journal* 44, 97–106.
- Boennohoff, K., 1980. 1,1-Diethoxyethane as diesel fuel. DE Patent no. 2 911, 411.
- Boennohoff, K., 1983. Method for enhancing the ignition performance of dialkoxyalkanes used as diesel fuel, in particular 1,1-diethoxyethane. DE Patent no. 3 136, 030.
- Boz, N., Dogu, T., Murtezaoglu, K., Dogu, G., 2004. Effect of hydrogen ion-exchange capacity on activity of resin catalysts in tert-amyl-ethyl-ether synthesis. *Applied Catalysis A* 268, 175–182.
- Bressa, S.P., Mariani, N.J., Ardiaca, N.O., Mazza, G.D., Martinez, O.M., Barreto, G.F., 2001. An algorithm for evaluating reaction rates of catalytic reaction networks with strong diffusion limitations. *Computers & Chemical Engineering* 25, 1185–1198.
- Caetano, N.S., Loureiro, J.M., Rodrigues, A.E., 1994. MTBE synthesis catalysed by acid ion exchange resins: kinetic studies and modeling of multiphase batch reactors. *Chemical Engineering Science* 49, 4589–4604.
- Carslaw, H.S., Jaeger, J.C., 1959. *Conduction of Heat in Solids*. Oxford University Press, Oxford, p. 102.
- Chaudhari, R.V., Mills, P.L., 2004. Multiphase catalysis and reaction engineering for emerging pharmaceutical processes. *Chemical Engineering Science* 59, 5337–5344.
- Da Silva, F., 1998. Personal Communication. Laboratory of Separation and Reaction Engineering, Faculty of Engineering, University of Porto.
- de Dardel, F., Arden, T.V., 2002. Ion exchangers. In: *Ullmann's Encyclopaedia of Industrial Chemistry*. Wiley-VCH, Weinheim (vol. Electronic Release).
- Dogu, T., Aydin, E., Boz, N., Murtezaoglu, K., Dogu, G., 2003. Diffusion resistances and contribution of surface diffusion in TAME and TAE production using Amberlyst-15. *International Journal of Chemical Reactor Engineering* 1, A6.
- Embree, H.D., Chen, T., Payne, G.F., 2001. Oxygenated aromatic compounds from renewable resources: motivation, opportunities, and adsorptive separations. *Chemical Engineering Journal* 84, 133–147.
- Ferreira, M.V., Loureiro, J.M., 2004. Number of active sites in TAME Synthesis: mechanism and kinetic modeling. *Industrial & Engineering Chemistry Research* 43, 5156–5165.
- Fite, C., Iborra, M., Tejero, J., Izquierdo, J.F., Cunill, F., 1994. Kinetics of the liquid-phase synthesis of ethyl tert-butyl ether ETBE. *Industrial & Engineering Chemistry Research* 33, 581–591.
- Fite, C., Tejero, J., Iborra, M., Cunill, F., Izquierdo, J.F., Parra, D., 1998. The effect of the reaction medium on the kinetics of the liquid-phase addition of the methanol to isobutene. *Applied Catalysis* 169, 165–177.
- Fredeslund, A., Gmehling, J., Rasmussen, P., 1977. *Vapor-Liquid Equilibria Using UNIFAC—A Group Contribution Method*. Elsevier, Amsterdam.
- Fredeslund, A., Jones, R.M., Prausnitz, J.M., 1998. Personal communication: supplement to program UNIFAC: group-contribution estimation of activity coefficients in nonideal liquid mixtures. Department of Chemical Engineering, University of California.
- Golubkov, A., Golubkov, I., 2002. Motor Fuel for diesel, gas-turbine and turbojet engines. US Patent no. 2002/0026744 A1.
- Ihm, S.K., Ahn, J.H., Jo, Y.D., 1996. Interaction of reaction and mass transfer in ion-exchange resin catalysts. *Industrial & Engineering Chemistry Research* 35, 2946–2954.
- IMSL, 1991. *IMSL STAT/LIBRARY User's Manual*. IMSL, Houston.
- Laborde, M.A., 2003. *Producción de Acetal a partir de Bioetanol*. Ediciones CYTED, Buenos Aires.
- Leitão, A., Dias, M., Rodrigues, A.E., 1994. Effectiveness of bidisperse catalysts with convective flow in the macropores. *Chemical Engineering Journal* 55, 81–86.
- Lode, F., Houmar, M., Migliorini, C., Mazzotti, M., Morbidelli, M., 2001. Continuous reactive chromatography. *Chemical Engineering Science* 56, 269–291.
- Lu, Z.P., Rodrigues, A.E., 1994. Pressure swing adsorption reactors: simulation of three-step one-bed process. *Separations* 40, 1118–1137.
- Lu, Z.P., Loureiro, J.M., LeVan, M.D., Rodrigues, A.E., 1992a. Dynamics of pressurization and blowdown of an adiabatic adsorption bed: 4. Intraparticle diffusion/convection models. *Gas Separation & Purification* 6, 89–100.
- Lu, Z.P., Loureiro, J.M., LeVan, M.D., Rodrigues, A.E., 1992b. Effect of intraparticle forced convection on gas desorption from fixed-beds containing large-pores adsorbents. *Industrial & Engineering Chemistry Research* 31, 1530–1540.
- Lu, Z.P., Loureiro, J.M., LeVan, M.D., Rodrigues, A.E., 1993a. Pressure swing adsorption process: intraparticle diffusion/convection models. *Industrial & Engineering Chemistry Research* 32, 2740–2752.
- Lu, Z.P., Loureiro, J.M., LeVan, M.D., Rodrigues, A.E., 1993b. Simulation of a three-step one-column pressure swing adsorption process. *A.I.Ch.E. Journal* 39, 1483–1496.
- Madsen, N.K., Sincovec, R.F., 1979. PDECOL: general collocation software for partial differential equations [D3]. *ACM Transactions on Mathematical Software* 5, 326–351.
- McGreavy, C., Draper, L., Kam, E.K.T., 1994. Methodologies for the design of reactors using structured catalysts: modelling and experimental study of diffusion and reaction in structured catalysts. *Chemical Engineering Science* 49, 5413–5425.
- Oktar, N., Murtezaoglu, K., Dogu, T., Dogu, G., 1999. Dynamic analysis of adsorption equilibrium and rate parameters of reactants and products in MTBE, ETBE and TAME production. *The Canadian Journal of Chemical Engineering* 77, 406–412.
- Oost, C., Hoffmann, U., 1996. The synthesis of tertiary amyl methyl ether (TAME): microkinetics of the reactions. *Chemical Engineering Science* 51, 329–340.
- Pääkkönen, P.K., Krause, A.O.I., 2003. Comparative study of TAME synthesis on ion-exchange resin beads and a fibrous ion-exchange catalyst. *Reactive & Functional Polymers* 55, 139–150.
- Paiva, A.L., Malcata, F.X., 1997. Reversible reaction and diffusion within a porous catalyst slab. *Chemical Engineering Science* 52, 4429–4432.
- Petersen, E.E., 1991. Adsorption in bidisperse-pore Systems. *A.I.Ch.E. Journal* 37, 671–678.
- Pöpken, T., Götz, L., Gmelhing, J., 2000. Reaction kinetics and chemical equilibrium of homogeneously and heterogeneously catalyzed acetic acid esterification with methanol and methyl acetate hydrolysis. *Industrial & Engineering Chemistry Research* 39, 2601–2611.
- Quinta-Ferreira, R.M., Rodrigues, A.E., 1993. Diffusion and catalytic zero order reaction in macroporous ion exchange resin. *Chemical Engineering Science* 48, 2927–2950.
- Quinta-Ferreira, R.M., Almeida-Costa, C.A., Rodrigues, A.E., 1996. Heterogeneous models of tubular reactors packed with ion-exchange resins: simulation of the MTBE synthesis. *Industrial & Engineering Chemistry Research* 35, 3827–3841.
- Rehfinger, A., Hoffmann, U., 1990. Kinetics of methyl tertiary butyl ether liquid phase synthesis catalyzed by ion exchange resin—I. Intrinsic rate expression in liquid phase activities. *Chemical Engineering Science* 45, 1605–1617.
- Reid, R.C., Prausnitz, J.M., Poling, B.E., 1987. *The Properties of Gases and Liquids*. McGraw-Hill, New York.
- Ruckenstein, E., Vaidyanathan, A.S., Youngquist, G.R., 1971. Sorption by solids with bidisperse pore structures. *Chemical Engineering Science* 26, 1305–1318.
- Ruthven, D.M., Loughlin, K.F., 1972. The diffusion resistance of molecular sieve pellets. *The Canadian Journal of Chemical Engineering* 50, 550–552.
- Silva, V.M.T.M., 2003. Diethylacetal synthesis in simulated moving bed reactor. Ph.D. Thesis, Faculty of Engineering, University of Porto.
- Silva, V.M.T.M., Rodrigues, A.E., 1999. Adsorption and diffusion in bidisperse pore structures. *Industrial & Engineering Chemistry Research* 38, 4023–4031.

- Silva, V.M.T.M., Rodrigues, A.E., 2001. Synthesis of diethylacetal: thermodynamics and kinetic studies. *Chemical Engineering Science* 56, 1255–1263.
- Silva, V.M.T.M., Rodrigues, A.E., 2002. Dynamics of a fixed-bed adsorptive reactor for synthesis of diethylacetal. *A.I.Ch.E. Journal* 48, 625–634.
- Sundmacher, K., Zhang, R.S., Hoffmann, U., 1995. Mass-transfer effects on kinetics of nonideal liquid-phase ethyl tert-butyl ether formation. *Chemical Engineering & Technology* 18, 269–277.
- Taqvi, S.M., Vishnoi, A., Levan, M.D., 1997. Effect of macropore convection on mass transfer in a bidisperse adsorbent particle. *Adsorption* 3, 127–136.
- Tartarelli, R., Conti, S., Capovani, M., 1970. On the second-order reactions in heterogeneous catalysis. *Catalysis Journal* 18, 212.
- Tirronen, E., Salmi, T., 2003. Process development in the fine chemical industry. *Chemical Engineering Journal* 91, 103–114.
- Turner, G.A., 1958. The flow structure in packed beds. *Chemical Engineering Science* 7, 156–165.
- Villermaux, J., Schweich, D., Authelin, J.R., 1987. Le Peigne du Diable: un modèle d'interface fractale bidimensionnelle. *Comptes Rendus de l'Académie des Sciences de Paris*, 304, série II, n° 8, 307–310.
- Wärnå, J., Rönholm, M.R., Salmi, T., Keikko, K., 2002. Influence of intraparticle reaction-diffusion in a catalytic reactor. *Chemical Engineering Journal* 90, 209–212.
- Zhang, T., Datta, R., 1995. Integral analysis of methyl tert-butyl ether synthesis kinetics. *Industrial & Engineering Chemistry Research* 34, 730–740.
- Ziyang, Z., Hidajat, K., Ray, A.K., 2001. Determination of adsorption and kinetic parameters for methyl tert-butyl ether synthesis from tert-butyl alcohol and methanol. *Journal of Catalysis* 200, 209–221.